Applied Catalysis A: General 525 (2016) 128–136

Contents lists available at ScienceDirect

Applied Catalysis A: General

journal homepage: www.elsevier.com/locate/apcata

Construction of graphite/TiO_2/nickel foam photoelectrode and its enhanced photocatalytic activity

Jialin Jia[a,b], Dong Li[a,b,*], Xiuwen Cheng[c], Jiafeng Wan[a,b], Xiujuan Yu[a,b,*]

[a] Department of Environmental Science and Engineering, Heilongjiang University, Xuefu Road 74, Nangang District, Harbin 150080, Heilongjiang Province, PR China
[b] Key Laboratory of Chemical Engineering Process & Technology for High-efficiency Conversion, Harbin, College of Heilongjiang Province, PR China
[c] Key Laboratory for Environmental Pollution Prediction and Control, Gansu Province, College of Earth and Environmental Sciences, Lanzhou University, Lanzhou 730000, PR China

ARTICLE INFO

Article history:
Received 14 May 2016
Received in revised form 11 July 2016
Accepted 17 July 2016
Available online 18 July 2016

Keywords:
TiO_2
Graphite
Nickel foam
Photoelectrode
Photoelectrocatalysis

ABSTRACT

Graphite/TiO_2/nickel foam photoelectrode was constructed through a modified sol-gel method, followed by coating procedure. Morphology, structure and optical property of the as-prepared photoelectrode was characterized via transmission electron microscopy (TEM), scanning electrons microscopy (SEM), X-ray photoelectron microscopy (XPS), X-ray diffraction (XRD) and UV–vis diffuse reflection spectroscopy (DRS). Results indicated that nickel foam framework was partly covered by graphite/TiO_2 and the crystallite sizes of anatase TiO_2 were found to be about 10 nm. C elements were incorporated into the lattice of TiO_2 nanoparticles through replacing titanium atom. Graphite/TiO_2/nickel foam photoelectrode showed the enhancement of light absorption in entire UV–vis regions. Besides, the photoelectrochemical performances of the graphite/TiO_2/nickel foam electrode were studied by transient photocurrent response (TPR), open circuit voltage (OCV) and electrochemical impedance spectroscopy (EIS). Moreover, photodecomposition properties of the electrode were evaluated by the generation of hydroxyl (•OH) radicals, photocatalytic (PC) and photoelectrocatalytic (PEC) degradation of methyl orange (MO). The graphite/TiO_2/nickel foam electrode revealed high transient photogenerated current of 0.054 $mAcm^{-2}$, open circuit photovoltage of −0.32 $mVcm^{-2}$, yield of •OH radicals, PC activity of 85.1% and PEC activity of 99.8% for removal of MO. The improved PEC efficiency could be mainly ascribed to the coupled graphite, nickel foam support and applied bias voltage, which could not only enhance the UV–vis light absorption, but also accelerate the charges separation and transfer.

1. Introduction

Titanium dioxide (TiO_2) has many unique features, such as low cost, nontoxicity, high thermal and chemical stabilities, abundance and high photo-oxidizing efficiency. These features make it become one of the most widely employed heterogeneous photocatalysts for solar energy conversion and environmental purification [1]. But there are still some shortcomings which limit its massive investment in practical applications, the most important three factors are as follows. Firstly, pure TiO_2 can merely be stimulated by ultraviolet light, which only occupies approximately 4% of the solar spectrum [2]. Secondly, the high recombination of photogenerated electron-hole pairs contributes to a low quantum efficiency, consequently reducing the PC activity of TiO_2 [3]. Thirdly, the pulverous TiO_2 photocatalyst is very difficult to separate and recycle in the suspending system.

To conquer the above defects, countless efforts have been made by predecessors. For the first two defects, a series of strategies have been carried out, such as depositing noble metals [4,5], coupling with polymers and narrow band gap semiconductors as well as carbon materials [6–10], photosensitization with dyes [11] and adulteration with non-metal or metal elements [12,13]. In recent years, the combination of TiO_2 nano-catalyst with carbon materials has received particular attention, this can be classified into the following three points: (a) Carbon materials can be used as a conductor to attract elections so as to improve the separation efficiency of photoexcited electron-hole pairs [14]. (b) Carbon materials can extend the light absorption of TiO_2 from the UV region to the visible-light region [15]. (c) C element in the carbon materials is always demonstrated transferring into the lattice of TiO_2 through replacing some lattice Ti atoms and forms Ti–O–C bond and can also produce a new impurity level through hybridization of C2p and O2p atomic orbits just above the valence band of TiO_2, thus improv-

* Corresponding authors.
E-mail addresses: lidong890210@126.com (D. Li), yuxiujuan@hlju.edu.cn (X. Yu).

http://dx.doi.org/10.1016/j.apcata.2016.07.010
0926-860X/

ing the utilization efficiency of visible light [16]. Among several carbon materials, such as carbon nanotubes [4,8], graphite [10,16], expanded graphite [17] and graphene [9], the graphite has become popular as its low cost, available, high temperature resistance, compatibility and the simple and large-scale produced relative to other counterparts [10,16]. Also, it is well known that photoelectrocatalysis is an efficient approach to promote the separation efficiency of photoinduced charge carriers.

Recently, to solve the issue of photocatalyst reclamation difficulty, various materials as supports for immobilizing pulverous photocatalyst have been used [18,19], including ceramic plate [20], glass plate [18], stainless steel plate [21], b-SiC foam [21], reactor wall [19] and nickel foam [22] etc. Among these, nickel foam as a functional material has high electronic conductivity and desirable three-dimensional cross-linked grid structure which can provide high porosity and surface area and strong adsorption ability, making it get more and more attention and be the more perfect support for catalyst loading [22–24]. Nickel foam with good adsorption performance can adsorb the more organic pollutants to its surface, this can increase the reactive area between the photocatalysts and the pollutants, moreover, its good plasticity make it become more flexible in the experimental process. Yuan et al. [22] prepared the Al_2O_3–SiO_2 interlayer and Pt loading on TiO_2/nickel-foam photocatalyst for degrading gaseous acetaldehyde, resulting in higher PC activity and stability of TiO_2 photocatalyst. Lei et al. [24] manufactured a three-dimensional NiAl-mixed metal oxide film electrode for an electrosorption application, in which the nickel foam was served as the substrate. The prepared NiAl-mixed metal oxide electrode displayed high electrosorption efficiency and good regeneration performance. Therefore, it is a considerable prospect to devise and exploit nickel foam-based support materials for practical application. Meanwhile, we deem that TiO_2 coupling with graphite immobilized on the nickel foam as photoelectrode was an effective and promising strategy to accomplish simultaneously superior light absorbability, electron transferability, separation ability from suspension and PC performance.

Hence, in our present work, the graphite/TiO_2 composite was synthesized by a modified sol-gel method, and then immobilized it on the nickel foam through coating approach. The morphology, structure, optical performance of the resulting material was characterized by TEM, SEM, XRD, XPS and DRS. Photoelectrochemical properties of the electrodes were investigated through transient photocurrent response (TPR), open circuit voltage (OCV) and electrochemical impedance spectroscopy (EIS). In addition, MO was chosen as the target pollutant to evaluate the PC and PEC activities of the graphite/TiO_2/nickel foam photoelectrode in aqueous solution. As a result, graphite/TiO_2/nickel foam photoelectrode exhibited superior charge separation efficiency and PC and PEC performance.

2. Experimental

2.1. Materials

Nickel foam (99.9%, PPI: 110) was purchased from Changsha Liyuan Material Co., Ltd. UV cut-off filter (LP420, 420 – 1100 nm with Transmittance (T) of 93% – 96%, 400 – 420 nm with T of 2% – 93%, Central wavelength at 410 ± 5 nm with T of 50%) was purchased from Shenzhen Nano Macro Photonics Technology Co., Ltd. All chemicals used in this study were of analytical grade, most of which were purchased from Sinopharm Chemical Reagent Co., Ltd, and distilled water was used throughout all our experiments.

2.2. Construction of graphite/TiO_2/nickel foam photoelectrode

Graphite/TiO_2 composites were constructed by simple one step sol-gel reaction according to our previous study [16]. Typically, a volume of 10 mL tetrabutyl titanate was added into 40 mL absolute ethanol under vigorous stirring to obtain solution A. Then, another solution B, which composed of deionized water, ethanol and HNO_3 with a volume ratio of 5:5:1 was added dropwise into the solution A under stirring, which denoted as solution C. After that, the desired amount of graphite (0.03 g) was immediately added into the solution C. The obtained mixture was intensively stirred for 150 min. The resulting black sol was aged for 24 h, and then dried at about 80 °C in oven for 48 h. At last, graphite/TiO_2 composite was obtained by calcination at 350 °C for 2 h. The mass ratio of graphite to TiO_2 in composite was approximately 1:78.

Graphite/TiO_2/nickel foam photoelectrode was prepared by coating graphite/TiO_2 and polytetrafluoroethylene (PTFE) composite, in which the nickel foam was served as the support. At room temperature, the diluted PTFE latex (10 wt%) as a binder and absolute ethanol as a dispersant were added dropwise and alternately into the beaker which contained a certain amount of graphite/TiO_2 under stirring constantly, and the mass ratio of graphite/TiO_2, PTFE and ethanol was 1:3:3. Then the graphite/TiO_2/nickel foam composite electrode was successfully obtained by coating the 0.2 g graphite/TiO_2-PTFE mixture (maximum loading) on the nickel foam repeatedly with a brush. Finally, the obtained graphite/TiO_2/nickel foam photoelectrode was dried in oven at 80 °C for 1 h to evaporate ethanol. As a comparison, pure TiO_2/nickel foam electrode was fabricated in the same method.

2.3. Characterization

The morphologies of the as-prepared graphite/TiO_2 and graphite/TiO_2/foam nickel were observed through transmission electron microscopy (JEOL JEM-2010) and field emission scanning electron microscope (FE-SEM, Hitachi S-4800). X-ray diffraction (XRD) patterns were recorded on a D8 Advance (Bruker) X-ray diffractometer with Cu Kα radiation. The accelerating voltage and applied current were held at 40 kV and 30 mA, respectively. X-ray photoelectron spectroscopy (XPS) data were measured on a Kratos AXIS Ultra DLD electron spectrometer. Fourier Transform Infrared spectra (FTIR) were recorded with a spectrum one spectrometer (PE) with KBr as diluents. Ultraviolet-visible diffuse reflectance spectra (UV-vis DRS) of the samples were conducted on a TU-1901 spectrophotometer with an integrating sphere attachment and $BaSO_4$ was used as the background ranging from 200 nm to 800 nm. Formation of hydroxyl (•OH) radicals at the photo-irradiated graphite/TiO_2/nickel foam photoelectrode/solution interface was measured via the fluorescence (FL) technique on a RF-5301PC fluorescence spectrophotometer.

2.4. Photoelectrochemical measurement

Transient photocurrent response and open circuit voltage of the as-prepared TiO_2/nickel foam and graphite/TiO_2/nickel foam photoelectrodes were measured on a CHI700e electrochemical workstation in a standard three-cell configuration in which TiO_2/nickel foam or graphite/TiO_2/nickel foam photoelectrode, Pt electrode and saturated calomel electrode (SCE) electrode were served as photoanode, counter electrode and reference electrode, respectively. Electrochemical impedance spectroscopy (EIS) plots were recorded in dark and under Xenon lamp irradiation with a frequency between 10^{-2} Hz and 10^5 Hz with or without an applied voltage. In this contribution, the supporting electrolyte was 0.1 molL^{-1} Na_2SO_4 solution.

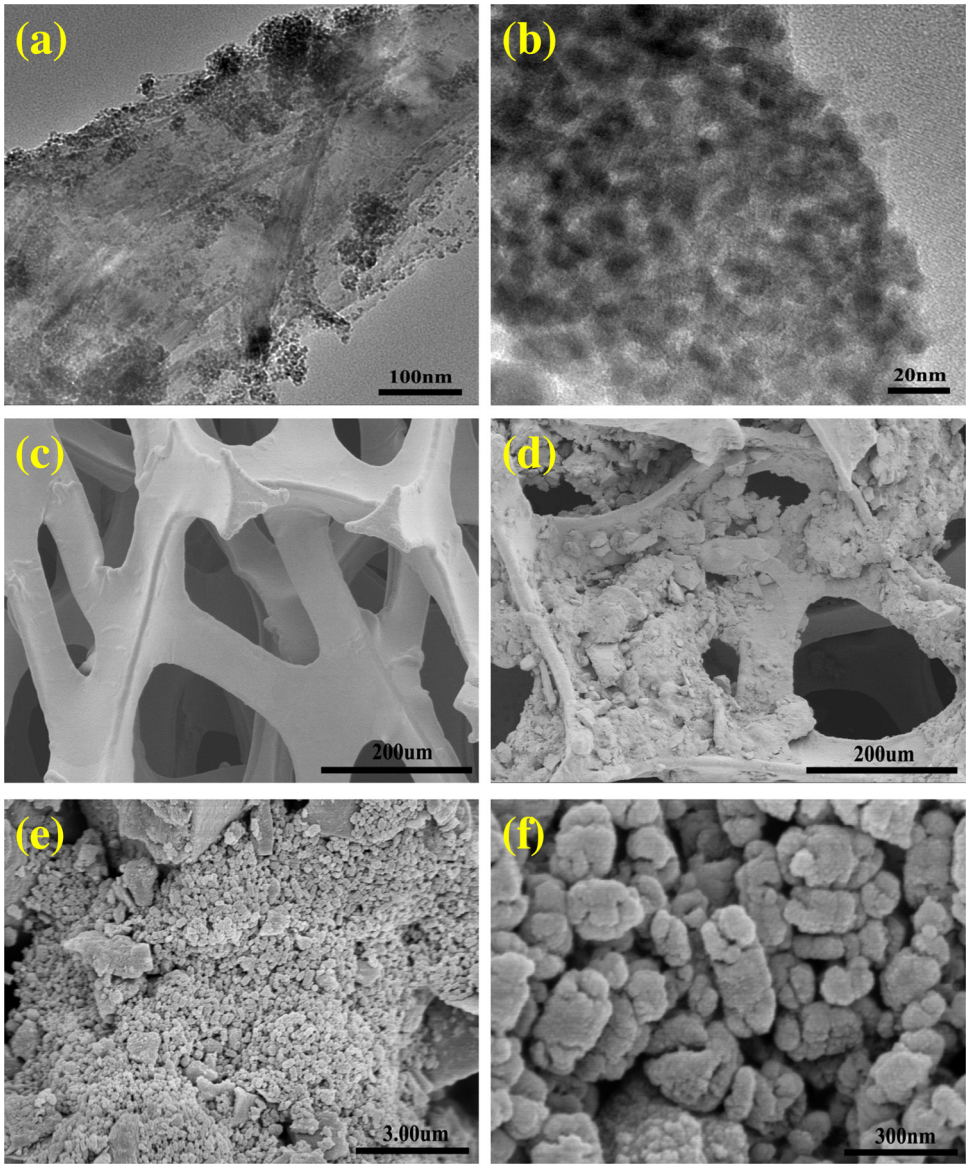

Fig. 1. TEM images of graphite/TiO_2 (a, b) and SEM images of nickel foam (c) and graphite/TiO_2/nickel foam (d, e, f).

2.5. PC and PEC activity

PC and PEC performances of as-prepared samples were investigated through the removal of methyl orange. PEC degradation processes were conducted in a homemade cylindrical quartz photoreactor, which contained 30 mL aqueous solution of methyl orange (10 mg/L) as the model wastewater. A 500 W Xenon arc lamp with a UV cut-off filter was used as the visible light source ($420\,nm < \lambda < 1100\,nm$) to keep an irradiation intensity of 16.4 Klux, which was placed 15 cm beside the light source. The distance between anode and cathode (Pt electrode) was 2 cm, and a 2 V external voltage was applied and controlled by a two-channel output DC power supply (DH1715A-5). Prior to irradiation, the as-prepared photoelectrodes were fixed in the quartz reactor and vertically immersed into the solution with the photoreaction areas of $2 \times 4\,cm^2$. Afterwards, 500 W Xenon light was switched on. At given time intervals, the collected samples were filtrated and measured at 464 nm using a T6 UV–vis spectrophotometer. It should be noted that the PC process of samples was carried out under the same procedure without a 2 V external voltage, and the removal of methyl orange through direct adsorption in dark was also carried out.

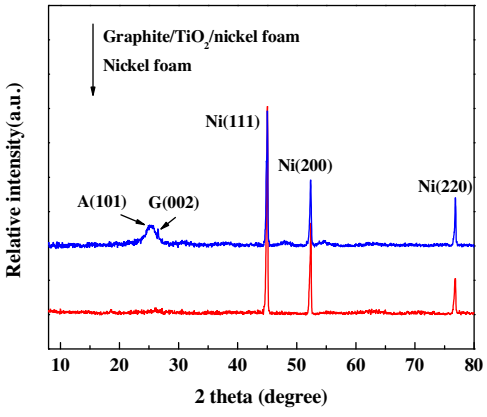

Fig. 2. XRD patterns of nickel foam and graphite/TiO_2/nickel foam.

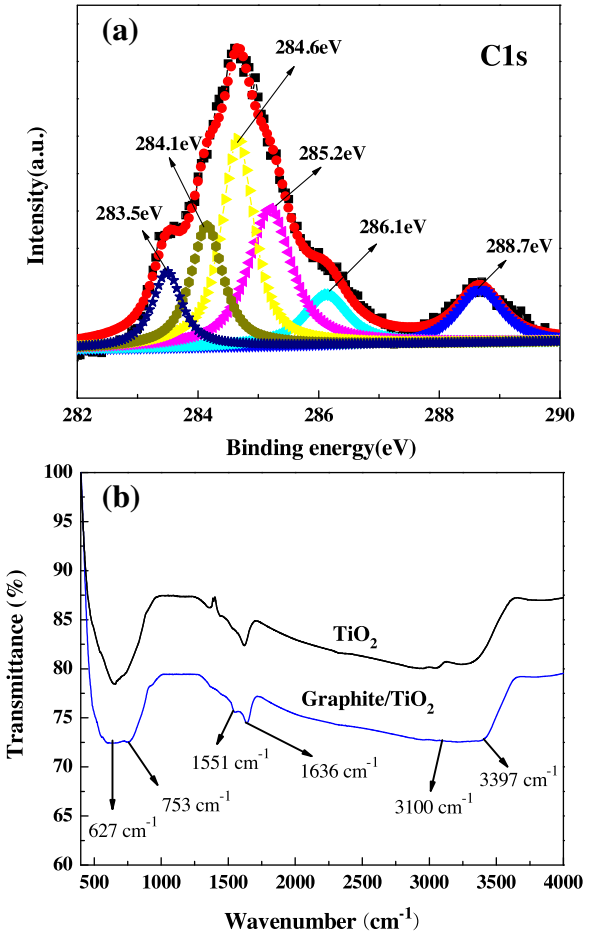

Fig. 3. High-resolution C1 s XPS spectrum (a) of graphite/TiO_2 composite and FTIR spectra (b) of pure TiO_2 and graphite/TiO_2 composite.

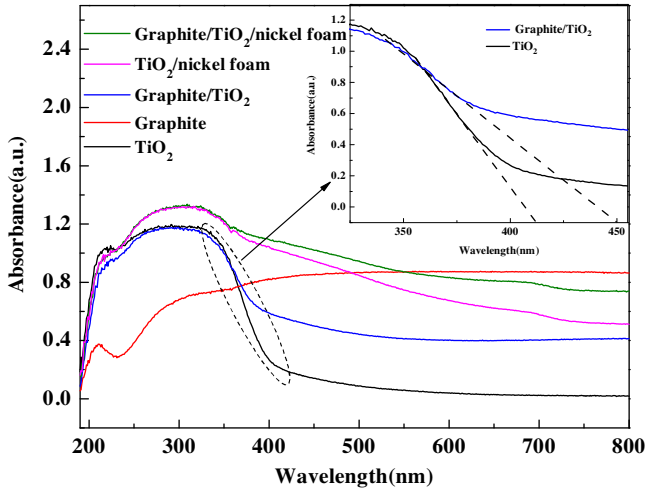

Fig. 4. UV–vis diffuse reflection spectra of the different samples.

3. Results and discussion

3.1. Characterization of the Graphite/TiO_2/nickel foam

The morphology of the graphite/TiO_2 composite and graphite/TiO_2/nickel foam photoelectrode were characterized by TEM and SEM. Fig. 1(a-b) displayed typical TEM images of as-prepared graphite/TiO_2 composite. Both the lamellate graphite and TiO_2 nanoparticle were visibly observed as shown in Fig. 1a. Distinctly, nanoscale TiO_2 particles were distributed uniformly on the surface of lamellate graphite. In Fig. 1b, it could be observed that TiO_2 particles displayed an equiaxed geometry and a small size distribution with average diameter of approximately 10 nm. Fig. 1c and Fig. 1d showed the SEM images of bare nickel foam and graphite/TiO_2/nickel foam photoelectrodes, which revealed a three-dimensional network structure. Nevertheless, as depicted in Fig. 1d, the hole of nickel foam framework were partly loaded by graphite/TiO_2 and PTFE composite, which coexisted with uncovered region of nickel foam. Magnified image (Fig. 1e) showed that the agglomerations of graphite/TiO_2 nanoparticles were formed and the graphite/TiO_2 nanoparticles composite become bigger particles under the action of the binder, and their diameters were ca. 150 nm, which consisted of primary particles with average diameter of 10 nm (Fig. 1f).

Fig. 2 revealed the XRD patterns of the nickel foam and graphite/TiO_2/nickel foam. As depicted in Fig. 2, the peaks located at 2θ value of 25.3° belonged to the (101) planes, this could be indexed to the anatase phase of TiO_2 (JCPDS file no. 21-1272). The diffraction peaks situated at 26.6° was the characteristics diffraction peak of (002) plane of graphite [25]. In addition, there were three strong and sharply peaks at 43.9, 51.5 and 75.8°, which were the diffraction peaks of nickel foam, which corresponded to the (111), (200) and (220) planes [26]. However, the pattern of graphite/TiO_2/nickel foam displayed no peak around 2θ = 12°, demonstrating inexistence of graphite oxide [27]. It was clearly evident from Fig. 2 that the XRD pattern of graphite/TiO_2/nickel foam composite depicted the diffraction peaks of graphite, anatase TiO_2 and nickel foam. It indicated that the graphite/TiO_2 composites were successfully loaded onto the nickel foam.

In order to investigate the chemical states of C element in the graphite/TiO_2/nickel foam composite, the typical XPS survey spectrum was employed, as shown in Fig. 3a. The C1 s peak could be deconvoluted into six peaks with Gaussian-Lorentzian rules at binding energy of 283.5 eV, 284.1 eV, 284.6 eV, 285.2 eV, 286.1 eV and 288.7 eV, respectively. The C1 s peak at binding energy of 283.5 eV had already been assigned to disordered graphite by previous investigator [28]. The two main peaks at 284.1 eV and 284.6 eV could be corresponded to sp^2 type C of graphite and adventitious carbon or C–C bond of the graphite [28–30], respectively, while another major peak at 285.2 eV was attributed to the presence of sp^3 type C graphitic component [28,29]. Furthermore, the other two peaks appeared at 286.1 eV and 288.7 eV could be assigned to C–O and Ti–O–C bond, respectively, which suggested that C was incorporated into the lattice of TiO_2 by substituting some of the lattice titanium atoms [14,31–33]. FTIR spectra of the TiO_2 and graphite/TiO_2 composite were conducted and displayed in Fig. 3b to support the XPS results. The strong peaks appearing at 3100–3400 cm^{-1} corresponded to the stretching vibrations of O–H bond [34,35]. The adsorption bands at around 1636 cm^{-1} were related to the H–O–H stretching vibrations of water, which were also ascribed to physisorbed water molecules on TiO_2 surface [35]. At 1551 cm^{-1} a C=C band of sp^2 hybridized carbons in graphite was observed for graphite/TiO_2 composite [36,37]. Compared with other papers [27,36,37], the lack of oxygen features (such as C=O bond at 1726 cm^{-1}, epoxide at 1230 cm^{-1} and carboxylates at 1050 cm^{-1} etc.) in the composite implied no formation of graphite oxide, correlating well with the XRD results. In the spectrum of TiO_2, the band at 643 cm^{-1} was associated with the stretching vibration of Ti–O–Ti bond and Ti–O bond. Typically, Ti–O–Ti (Ti–O) and Ti–O–C stretching vibrations exhibited low frequency bands around (625–690) cm^{-1} and 798 cm^{-1}, respectively [33,36,38]. Thus, the broad bands at the low frequency region (627–753 cm^{-1}) in the graphite/TiO_2 composite could be considered a combination of Ti–O–Ti and Ti–O–C stretching vibrations due

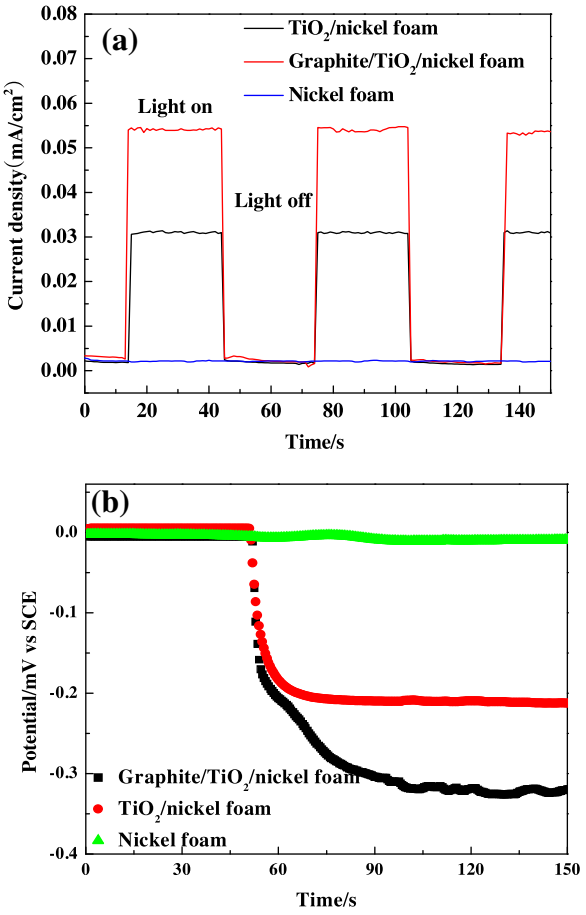

Fig. 5. Transient photocurrent response (a) and open circuit voltage (b) of the nickel foam, TiO_2/nickel foam and graphite/TiO_2/nickel foam photoelectrodes.

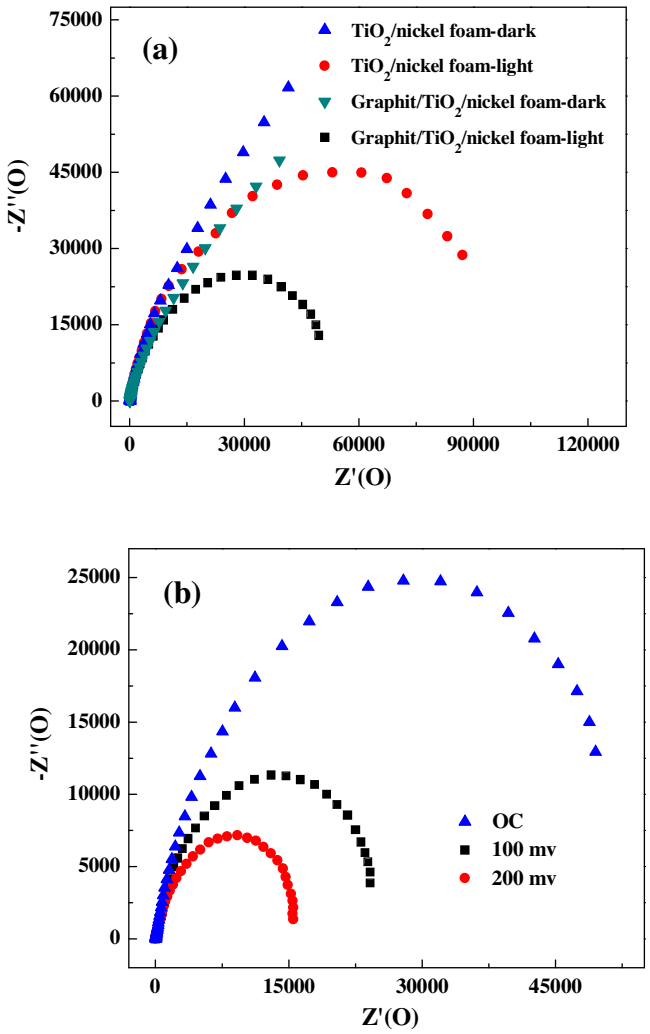

Fig. 6. (a) EIS Nyquist plots at open circuit voltage in dark and under Xenon lamp illumination of the TiO_2/nickel foam and graphite/TiO_2/nickel foam photoelectrodes. (b) Effect of external voltage on the EIS response of the graphite/TiO_2/nickel foam photoelectrode under Xenon lamp illumination.

to the chemical interaction of TiO_2 with the graphite [33,36,38]. The above analysis confirmed the successful chemical-coupling of TiO_2 and graphite.

Fig. 4 depicted the UV–vis DRS of the graphite/TiO_2/nickel foam, TiO_2/nickel foam, graphite/TiO_2, TiO_2 and graphite samples. As displayed in Fig. 4, it could be observed that the former four samples displayed inherent absorption spectra in the UV region, corresponding to the intrinsic band gap of pure TiO_2 [39]. The graphite sample revealed strong photo absorption over the entire visible light region. The pure TiO_2 exhibited a little visible light absorption. Nevertheless, compared with the pure TiO_2, the graphite/TiO_2 composite exhibited an improved absorption in the whole visible light region because of the photo-absorption property of the incorporation of graphite. As shown in the inset of Fig. 4, a slightly shift to visible light region was observed for the absorption edge of graphite/TiO_2 composite, which could be ascribed to the Ti–O–C bonds in the as-synthesized graphite/TiO_2 composite [16,40,41]. The tangent drawn exhibited an absorbance maximum of 413 nm for the TiO_2 and 449 nm for graphite/TiO_2 composite, corresponding to a band gap of 3.00 eV and 2.76 eV, respectively. Similar enhanced visible light absorption and shift for graphite/TiO_2 composite had been confirmed by our group [16,42]. In addition, the photo-absorption characteristic for TiO_2/nickel foam and graphite/TiO_2/nickel foam followed the same tendency with the pristine TiO_2 and the graphite/TiO_2 composite. But the slight shift to visible light wasn't obvious for the absorption edge of graphite/TiO_2/nickel foam. The photocatalysts immobilized on the nickel foam (graphite/TiO_2/nickel foam and TiO_2/nickel foam) showed a distinctly stronger absorption both in the ultraviolet light region and visible light region in comparison to the powder photocatalyst (graphite/TiO_2 and TiO_2). These might be attributed to effect of light absorption of the nickel foam. Therefore, it could be concluded that graphite/TiO_2/nickel foam electrode should reveal high PC activity.

3.2. Photoelectrochemical performances

Transient photocurrent responses (TPR) of the nickel foam, TiO_2/nickel foam and graphite/TiO_2/nickel foam photoelectrodes were conducted via several on-off cycles of Xenon lamp irradiation to investigate the separation efficiency of the photoexcited electron-hole pairs. In dark state, both the nickel foam photoelectrodes had no photocurrent response, as displayed in Fig. 5a. But the photocurrent response produced rapidly and augmented greatly as soon as the Xenon lamp was switched on and illuminated the surface of photoelectrodes, afterwards gradually smooth and steady, and attain a changeless value, this meant that photocurrent was fully thanks to the photo-activity of the photoelectrodes, and the charges migration were very quickly. Furthermore, the transient photocurrent density of graphite/TiO_2/nickel foam photoelectrode was approximately 0.054 $mAcm^{-2}$, higher than for TiO_2/nickel foam (0.031 $mAcm^{-2}$) electrode by a factor of

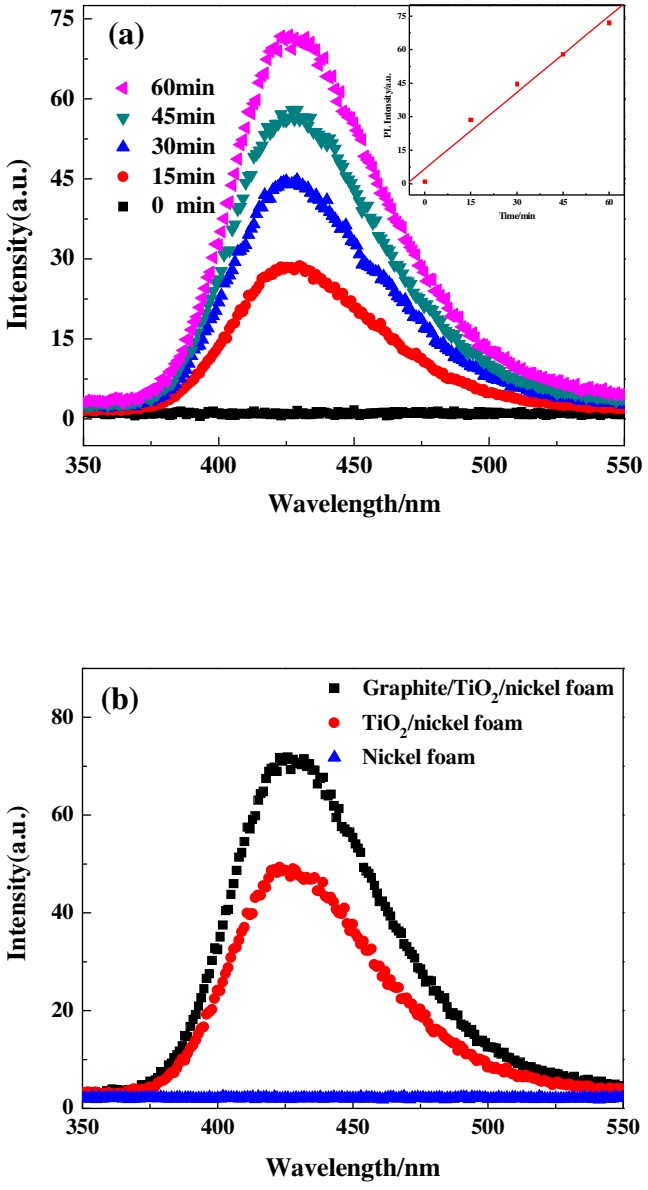

Fig. 7. (a) PL spectra evolutions as Xenon lamp illumination time over the graphite/TiO_2/nickel foam photoelectrode; (b) Comparative PL spectra on different electrode at a stated 60 min.

1.74 under Xenon lamp illumination, implying that chemical-coupling with graphite could markedly promote the separation of the photoexcited electrons and holes (e^-–h^+) pairs of TiO_2. Meanwhile, open circuit voltages (OCV) of the TiO_2/nickel foam and graphite/TiO_2/nickel foam photoelectrodes were measured to further investigate the influence of graphite on the property of photoexcited charge separation. As displayed in Fig. 5b, both TiO_2/nickel foam photoelectrodes revealed obviously increased OCV at the initial time of illumination, and then reached a constant voltage state after a period of time continuous irradiation, suggesting that photoexcited electrons transferred to and accumulated within the photoelectrode film [43]. Noticeably, it was clearly observed that graphite/TiO_2/nickel foam photoelectrode displayed a higher photovoltage ($-0.32\ mVcm^{-2}$) than for TiO_2/nickel foam electrode ($-0.21\ mVcm^{-2}$), implying that graphite could induce the accumulation of more electrons in graphite/TiO_2/nickel foam photoelectrode interior. Moreover, no matter the dark or light conditions, pure nickel foam neither showed the TPR nor the OCV response. Therefore, it could be con-

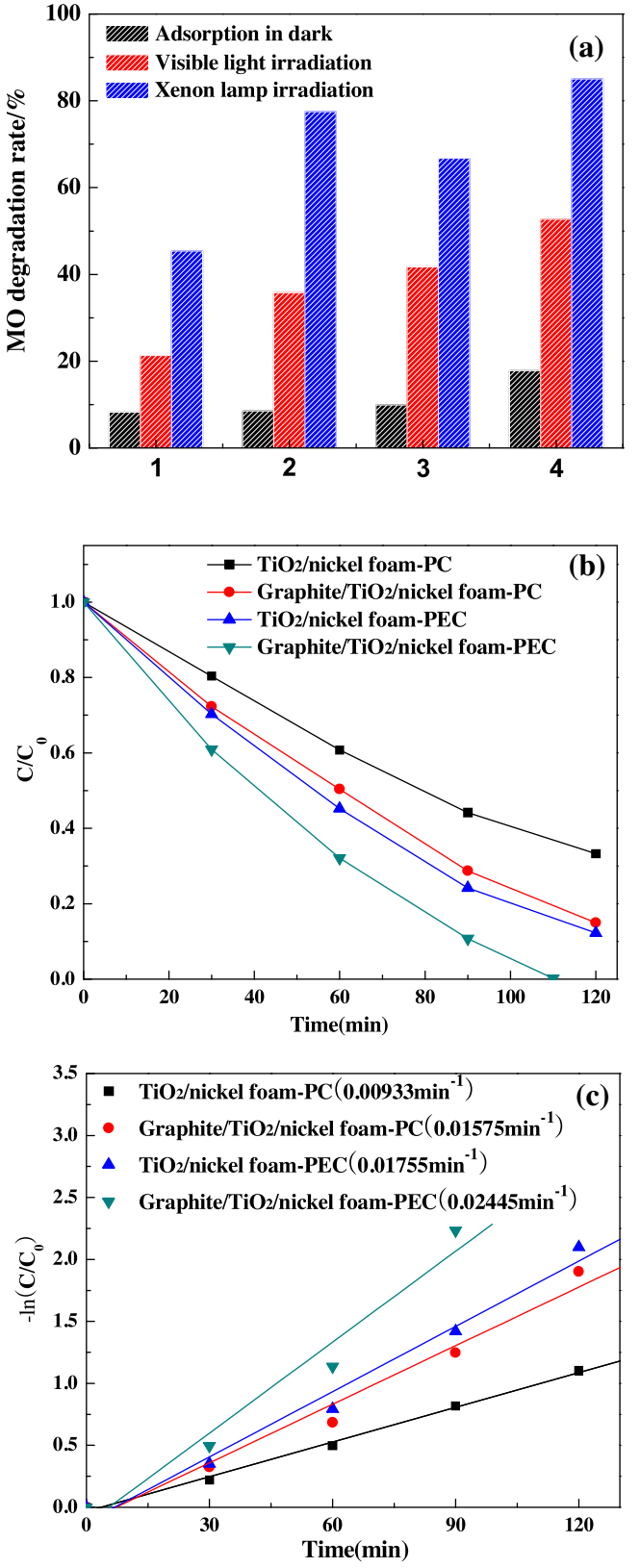

Fig. 8. PC removal of MO over (1) home-made TiO_2, (2) graphite/TiO_2, (3) TiO_2/nickel foam photoelectrode and (4) graphite/TiO_2/nickel foam photoelectrode under various conditions (a); PC and PEC degradation efficiency (b) and kinetic linear fitting curves (c) of MO aqueous solution over as-prepared TiO_2/nickel foam and graphite/TiO_2/nickel foam electrodes.

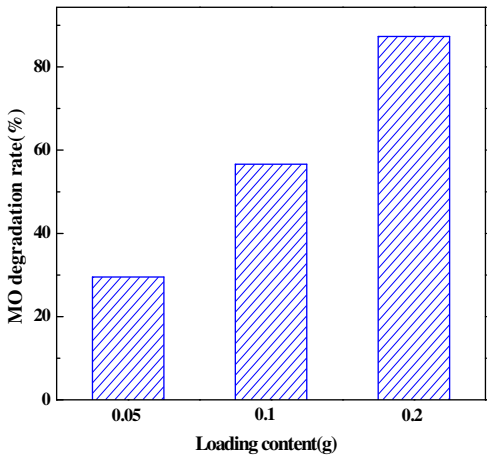

Fig. 9. PC degradation of MO on graphite/TiO_2/nickel foam electrode with different graphite/TiO_2 loading.

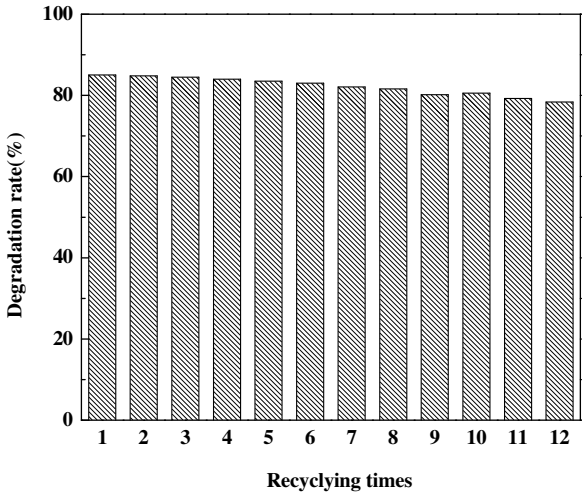

Fig. 10. Repeated utilization of graphite/TiO_2/nickel foam photoelectrode for PC degradation of MO.

cluded that graphite/TiO_2/nickel foam photoelectrode performed an effective separation of photoexcited charge carriers, which was in accordance with the photocurrent performance.

Electrochemical impedance spectroscopy (EIS) is an powerful approach to investigate the photoexcited charges transport and recombination processes of TiO_2 photoelectrode in the PC and PEC reaction [44]. Fig. 6 displayed typical EIS Nyquist plots of the graphite/TiO_2/nickel foam and TiO_2/nickel foam photoelectrodes at open circuit voltage (OCV) under dark and Xenon lamp illumination. Clearly, the circular arc radius of the EIS Nyquist plots distinctly reduced with the Xenon lamp illuminated, as shown in Fig. 6a, implying that the photo-excited electrons and holes pairs could be effectively separated and transferred and resistance of electron transport commanded the kinetics at the photoelectrode interface [45,46]. Besides, regardless of in dark or under Xenon lamp illumination, it should be noticed that the arc radius on the Nyquist plots of graphite/TiO_2/nickel foam was lesser than that of TiO_2/nickel foam, manifesting that the charge transport resistance decreased after the incorporation of graphite, which was on account of that coupled graphite as appropriate electronic conductors significantly promoted the separation of photoexcited charge carriers via attracting and expediting interfacial transport of electrons. Noticeably, the arc radius obviously decreased with the assistance of external voltage, meaning that photoexcited hole-electron (h^+/e^-) pairs were more efficiently separated and transferred as seen from Fig. 6b. As known, the hydroxyl radicals (•OH) generated have been regarded as the dominant reactive species responsible towards the PC and PEC degradation processes [47]. Hence, to evaluate the PC activity of the graphite/TiO_2/nickel foam photoelectrode, the production of •OH at photo-irradiated photoelectrode/solution interface had been measured through recording the fluorescence derived from the reactions between •OH radicals and terephthalic acid (TA) to produce 2-hydroxyterephthalic acid with a high fluorescent characteristic peak at approximately 425 nm [48]. Fig. 7a presented the comparison of PL intensity of generated TAOH using graphite/TiO_2/nickel foam electrode in 5×10^{-4} mol L^{-1} TA solution under Xenon light irradiation as illumination time. Distinctly, it is evident from results that the PL peak located at ca. 425 nm improved gradually as prolonging illumination time over the graphite/TiO_2/nickel foam photoelectrode. The intensity of PL peak around 425 nm augmented linearly as illumination time (as depicted in the inset of Fig. 7a), implying that the output of •OH generated over the graphite/TiO_2/nickel foam electrode was proportional to the illumination time. Whereas, no PL peaks were measured for the pure nickel foam or in the absence of the light illumination (Fig. 7b) of TiO_2/nickel foam and graphite/TiO_2/nickel foam photoelectrode. Fig. 7b also revealed the comparative fluorescence intensity of TAOH over the graphite/TiO_2/nickel foam and TiO_2/nickel foam photoelectrodes at a stated 60 min under simulated sunlight illumination. Markedly, graphite/TiO_2/nickel foam electrode displayed the higher intensity of PL signal at 425 nm than TiO_2/nickel foam, suggesting that the productivity of •OH radicals over the graphite/TiO_2/nickel foam photoelectrode was stronger than that of TiO_2/nickel foam, which should be attributed to the coupled graphite. For one thing, graphite could adequately arouse the more intense light absorption, thus producing more •OH radicals output. For another, the coupled graphite could improve the separation efficiency of photoexcited charge carriers of TiO_2, consequently contributing to a longer lifetime of photoexcited electrons and holes. The higher PC activity of the graphite/TiO_2/nickel foam photoelectrode should be anticipated.

3.3. PC and PEC activity

To investigate the PC and PEC activities of the as-prepared TiO_2/nickel foam and graphite/TiO_2/nickel foam photoelectrodes, degradation of methyl orange aqueous solution were performed under visible light and Xenon lamp irradiation. The PC efficiency of pulverous TiO_2 catalysts, which was equivalent to the amount of coating on nickel foam support, was also conducted as a reference. In our contribution, only a small amount of methyl orange (<3%) could be removed via direct photolysis compared to the PC and PEC degradation, which was negligible. As depicted in Fig. 8a, the removal efficiency of MO resulted from adsorption in dark over TiO_2/nickel foam within 120 min was 9.9%, a slightly higher than for home-made pulverous TiO_2 (8.2%), while the adsorption of MO on graphite/TiO_2/nickel foam electrode (17.8%) was 2.1 times the value (8.5%) obtained using graphite/TiO_2, which might be attributed to the adsorption ability for contaminants of the nickel foam. Under Xenon light irradiation, the photocataltytic activities of TiO_2/nickel foam (66.7%) and graphite/TiO_2/nickel foam (85.1%) were higher than that of home-made TiO_2 (45.4%) and graphite/TiO_2 composite (77.5%), respectively. Also, a higher removal rate of MO was achieved upon using TiO_2/nickel foam (41.7%) and graphite/TiO_2/nickel foam (52.7%) under visible (>420 nm) light irradiation. These might be attributed to the intense visible light response of the nickel foam. As observed from Fig. 8a and b, the removal efficiency of methyl orange

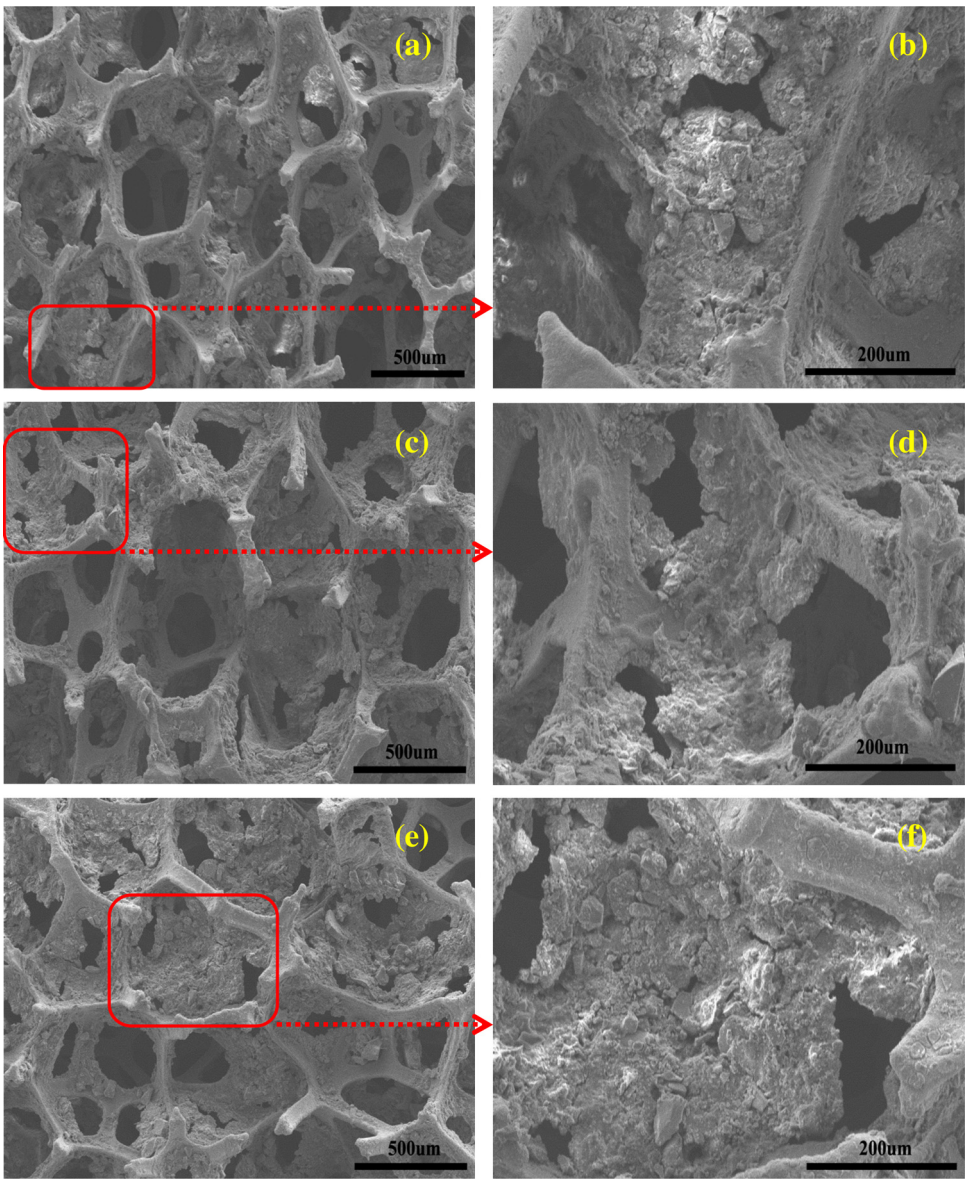

Fig. 11. SEM images (a, b, c, d, e, f) of graphite/TiO_2/nickel foam photoelectrode after twelve cycles for PC degradation of MO. (All of the images were the same sample).

could be improved by the coupling with graphite, which was supported by the results of PL, DRS and photoelectrochemical. And both of the PC and PEC efficiency of the as-prepared TiO_2/nickel foam and graphite/TiO_2/nickel foam electrodes could be arranged in the following sequence: graphite/TiO_2/nickel foam-PEC > TiO_2/nickel foam-PEC > graphite/TiO_2/nickel foam-PC > TiO_2/nickel foam-PC. Namely, graphite/TiO_2/nickel foam photoelectrode exhibited highest PC and PEC activity, for which 85.1% (within 120 min) and 99.8% (within 110 min) of methyl orange could be degraded, respectively, which could be attributed to the following four aspects: (a) Combination of TiO_2 and graphite generated Ti–O–C bonds, which could narrow the band gap of TiO_2 thereby utilizing the visible light. (b) Nickel foam support and coupled graphite enhanced light absorption capacity of TiO_2 both in UV and visible regions. (c) Incorporated graphite accelerated the electrons transport and transfer. (d) Applied external voltage promoted the migration of photoexcited electrons from as-prepared photoanode to the Pt electrode hence further preventing the charge carrier (electron-hole pairs) recombination.

Meanwhile, the experimental data of PC and PEC removal of methyl orange under Xenon lamp irradiation were found to approximately fit the pseudo-first order kinetics formula according to the linear transforms $-\ln(C/C_0)|f(t) = kt$(k is kinetic constant) based on Langmuir-Hinshelwood model within 120 min [49], as shown in Fig. 8c. The corresponding kinetic constants of both nickel foam photoelectrodes were exhibited in the parentheses of Fig. 8c and could be arranged in the following sequence: graphite/TiO_2/nickel foam-PEC > TiO_2/nickel foam-PEC > graphite/TiO_2/nickel foam-PC > TiO_2/nickel foam-PC. Noticeably, graphite/TiO_2/nickel foam photoelectrode depicted the outstanding PEC performance with the highest kinetic constant of 0.02445 min^{-1}. The superior PEC activity could be ascribed to the intense light absorption ability and effective charge separation and transfer.

Fig. 9 showed the PC degradation of MO on graphite/TiO_2/nickel foam photoelectrode with different supported amount of graphite/TiO_2 composite. The degradation efficiency of MO increased from 29.5% to 56.6% when the loading of graphite/TiO_2

was increased from 0.05 g to 0.1 g. Further increasing graphite/TiO_2 composite content to 0.2 g (maximum amount) could improve the removal efficiency of MO to 85.1%. The increase of graphite/TiO_2 loading could contribute to generate more reaction active sites. As a result, the light could be utilized effectively to participate in the PC process, resulting in a high PC activity.

Reusability is an important consideration for the practical application of photocatalysts in water remediation. Hence, the PC stability of graphite/TiO_2/nickel foam electrode was investigated by repeating the PC degradation of methyl orange under Xenon lamp irradiation for 120 min (Fig. 10). It could be seen that after twelve cycles the PC degradation efficiency of graphite/TiO_2/nickel foam decreased from 85.1 to 78.3%. The SEM images of the graphite/TiO_2/nickel foam electrode after twelve cycles were provided in Fig. 11. All of the six SEM images exhibited the same sample. Fig. 11b, Fig. 11d and Fig. 11f showed the magnification of approximate area from Fig. 11a, Fig. 11c and Fig. 11e outlined in red rectangle, respectively. The graphite/TiO_2 composites were still stabilized on the surfaces and holes of nickel foam after twelve cycles. These demonstrated that the graphite/TiO_2/nickel foam possesses high activity stability and may be adopted as practically viable and stable photoelectrode.

4. Conclusions

In summary, graphite/TiO_2/nickel foam photoelectrode had been successfully manufactured by a facile sol-gel and coating strategy, and applied to PC and PEC degradation of MO. The morphology, structure, optical performance and photoelectrochemical property of graphite/TiO_2/nickel foam photoelectrode was investigated through a series of characterizations, and discussed in detail. Results indicated that the incorporation of graphite could enhance visible light absorption and promote the separation of the photoexcited electrons and holes. Also, nickel foam support could not only further improve the UV–vis light absorption of graphite/TiO_2, but also adsorb more organic pollutants. Most important, it was an excellent support to immobilize the pulverous TiO_2. The as-prepared graphite/TiO_2/nickel foam photoelectrode depicted intense absorption both in ultraviolet and visible light regions, high TPR of 0.054 $mAcm^{-2}$ and OCV of −0.32 $mVcm^{-2}$ as well as low electrons transport resistance. Furthermore, it also possessed excellent PC activity of 85.1% and PEC activity of 99.8% for degrading organic pollutants (MO) under Xenon light irradiation. The high-efficiency PC and PEC activity could be ascribed to that the coupled graphite, nickel foam support and applied bias voltage improved the UV–vis light absorption and accelerated the charge separation and transfer. This study provides that graphite/TiO_2 composite anchored on nickel foam prepared by a simple method will be a promising material for PC and PEC water remediation applications.

Acknowledgments

This work was supported by National Natural Science Foundation of China for Youth (21106035) and Youth Scholar Backbone Supporting Plan Project for General Colleges and Universities of Heilongjiang province (1151G034), and Key Laboratory of Chemical Engineering Process & Technology for High-efficiency Conversion.

References

[1] A. Fujishima, K. Honda, Nature 238 (1972) 37–38.
[2] S.A. Ansari, M.M. Khan, M.O. Ansari, M.H. Cho, Sol. Energy Mater. Sol. Cells 141 (2015) 162–170.
[3] J. Di, S. Li, Z. Zhao, Y. Huang, Y. Jia, H. Zheng, Chem. Eng. J. 281 (2015) 60–68.
[4] A. Pintar, M. Besson, P. Gallezot, Appl. Catal. B: Environ. 31 (2001) 275–290.
[5] M. Bowker, P. Stone, R. Bennett, N. Perkins, Surf. Sci. 511 (2002) 435–448.
[6] E. Filippo, C. Carlucci, A.L. Capodilupo, P. Perulli, F. Conciauro, G.A. Corrente, G. Gigli, G. Ciccarella, Appl. Surf. Sci. 331 (2015) 292–298.
[7] M.L. Zhong, G.Q. Zhang, X.Q. Yang, Mater. Lett. 145 (2015) 216–218.
[8] A. Kongkanand, P.V. Kamat, ACS Nano 1 (2007) 13–21.
[9] M. Ouzzine, A.J. Romero-Anaya, M.A. Lillo-Roídenas, A. Linares-Solano, Carbon 67 (2014) 104–118.
[10] G. Palmisano, V. Loddo, H.H. El Nazer, S. Yurdakal, V. Augugliaro, R. Ciriminna, M. Pagliaro, Chem. Eng. J. 155 (2009) 339–346.
[11] M. Liang, J. Chen, Chem. Soc. Rev. 42 (2013) 3453–3488.
[12] H.Q. Jiang, Q.Y. Wang, S.Y. Zang, J.S. Li, Q.F. Wang, J. Hazard. Mater. 261 (2013) 44–54.
[13] W. Choi, A. Termin, M.R. Hoffman, J. Phys. Chem. 98 (1994) 13669–13679.
[14] Y. Zhang, Z. Zhao, J. Chen, L. Cheng, J. Chang, W. Sheng, C. Hu, S. Cao, Appl. Catal. B: Environ. 165 (2015) 715–722.
[15] S. Lee, Y. Lee, D.H. Kim, J. Moon, ACS Appl. Mater. Interfaces 5 (2013) 12526–12532.
[16] J.L. Jia, D. Li, J.F. Wan, X.J. Yu, J. Ind. Eng. Chem. 33 (2016) 162–169.
[17] Y.M. Yu, N.Q. Zhao, C.S. Shi, C.N. He, E.Z. Liu, J.J. Li, Int. J. Hydrogen Energy 37 (2012) 5762–5768.
[18] M. Fathinia, A.R. Khataee, M. Zarei, S. Aber, J. Mol. Catal. A: Chem. 333 (2010) 73–84.
[19] M. Mehrjouei, S. Müller, D. Möller, Chem. Eng. J. 211-212 (2012) 353–359.
[20] M. Fathinia, A. Khataee, Appl. Catal. A: Gen. 491 (2015) 136–154.
[21] P. Rodriguez, V. Meille, S. Pallier, M.A.A. Sawah, Appl. Catal. A: Gen. 360 (2009) 154–162.
[22] J. Yuan, H. Hu, M.X. Chen, J.W. Chi, W.F. Shangguan, Catal. Today 139 (2008) 140–145.
[23] Y.L. Wang, Y.Q. Zhao, C.L. Xu, D.D. Zhao, M.W. Xu, Z.X. Su, H.L. Li, J. Power Source 195 (2010) 6496–6499.
[24] X.D. Lei, B. Wang, J.F. Liu, Z.P. Ye, Z. Chang, M.H. Jiang, X.M. Sun, RSC Adv. 4 (2014) 41642–41648.
[25] H. Panjiar, R.P. Gakkhar, B.S.S. Daniel, Powder Technol. 275 (2015) 25–29.
[26] F. Yang, B. Cao, Y. Tao, M. Hu, C.C. Feng, L. Wang, Z. Jiang, D.X. Cao, Ying Zhang, J. Power Sources 298 (2015) 38–45.
[27] T.S. Jiang, Z.F. Tao, M.R. Ji, Q. Zhao, X.Q. Fu, H.B. Yin, Catal. Commun. 28 (2012) 47–51.
[28] T. Paulmier, J.M. Bell, P.M. Fredericks, Thin Solid Films 515 (2007) 2926–2934.
[29] X.C. LeQuan, W.P. Kang, J.L. Davidson, B.K. Choi, Y.M. Wong, R. Barbosa, W. Lu, Diamond Relat. Mater. 18 (2009) 200–205.
[30] O. Akhavan, M. Abdolahad, A. Esfandiar, M. Mohatashamifar, J. Phys. Chem. C 114 (2010) 12955–12959.
[31] D. Li, Z.P. Xing, X.J. Yu, X.W. Cheng, Electrochim. Acta 170 (2015) 182–190.
[32] I.A. Appavoo, J. Hu, Y. Huang, S.F.Y. Li, S.L. Ong, Water Res. 57 (2014) 270–279.
[33] D. Li, J.L. Jia, Y.H. Zhang, N. Wang, X.L. Guo, X.J. Yu, J. Hazard. Mater. 315 (2016) 1–10.
[34] G.S. Li, L.P. Li, J. Boerio-Goates, B.F. Woodfield, J. Am. Chem. Soc. 127 (2005) 8659–8666.
[35] S.W. Liu, J.G. Yu, W.G. Wang, Phys. Chem. Chem. Phys. 12 (2010) 12308–12315.
[36] S.D. Perera, R.G. Mariano, K. Vu, N. Nour, O. Seitz, Y. Chabal, K.J. Balkus, Jr., ACS Catal. 2 (2012) 949–956.
[37] L. Zhu, S.B. Jo, S. Ye, K. Ullah, Z.D. Meng, W.C. Oh, J. Ind. Eng. Chem. 22 (2015) 264–271.
[38] H. Zhang, X.J. Lv, Y.M. Li, Y. Wang, J.H. Li, ACS Nano 4 (2010) 380–386.
[39] X.W. Cheng, X.J. Yu, Z.P. Xing, Mater. Res. Bull. 47 (2012) 3804–3809.
[40] Y.H. Zhang, Z.R. Tang, X.Z. Fu, Y.J. Xu, ACS Nano 4 (2010) 7303–7314.
[41] Y. Zhang, Z. Zhou, T. Chen, H. Wang, W. Lu, J. Environ. Sci. 26 (2014) 2114–2122.
[42] X.J. Yu, Y.H. Zhang, X.W. Cheng, Electrochim. Acta 137 (2014) 668–675.
[43] B.H. Meekins, P.V. Kamat, ACS Nano 3 (2009) 3437–3446.
[44] F. Fabregat-Sntiago, E.M. Barea, J. Bisquert, G.K. Mor, K. Shankar, C.A. Grimes, J. Am. Chem. Soc. 130 (2008) 11312–11316.
[45] S.N. Chai, G.H. Zhao, Y.N. Zhang, Y.J. Wang, F.Q. Nong, M.F. Li, D.M. Li, Environ. Sci. Technol. 46 (2012) 10182–10190.
[46] X. Zhao, Y.F. Zhu, Environ. Sci. Technol. 40 (2006) 3367–3372.
[47] D. Li, X.W. Cheng, X.J. Yu, Z.P. Xing, Chem. Eng. J. 279 (2015) 994–1003.
[48] Y.Y. Song, P. Roy, I. Paramasivam, P. Schmuki, Angew. Chem. Int. Ed. 49 (2010) 351–354.
[49] D. Li, J.L. Jia, T. Zheng, X.W. Cheng, X.J. Yu, Appl. Catal. B: Environ. 188 (2016) 259–271.